THE ASTROPHYSICAL JOURNAL, 241:374–384, 1980 October 1

ON THE FORMATION OF Fe II LINES IN STELLAR SPECTRA. I. SOLAR SPATIAL INTENSITY VARIATION OF λ3969.4

LAWRENCE E. CRAM AND ROBERT J. RUTTEN[1]
Sacramento Peak Observatory[2]

AND

BRUCE W. LITES
Laboratory for Atmospheric and Space Physics
Received 1979 December 17; accepted 1980 March 28

ABSTRACT

We employ high–spatial-resolution solar observations of the weak Fe II λ3969.4 line to study non–local thermodynamic equilibrium (NLTE) effects in Fe II line formation. This line is superposed on the wing of the Ca II H line, which raises its height of formation. The line shows extraordinary spatial intensity variations, including emission features whose contrast increases toward the limb. Observed profiles of the Fe II resonance lines in the UV are used to define formation parameters in a 15-level atomic model computation, which shows that Fe II subordinate lines are generally formed out of local thermodynamic equilibrium (LTE) as a result of pumping by UV line-wing photons from the deep photosphere. For the λ3969.4 line, this pumping results in large sensitivity to the atmospheric structure in layers *deeper* than the layer of formation of the H-wing background intensity. We discuss the absence of intense emission cores in the Fe II resonance lines, the effects of partially coherent scattering, and the effects of chromospheric and photospheric inhomogeneities. We find that emission of λ3969.4 provides a diagnostic of the inhomogeneous structure of the deep photosphere, for the Sun and for late-type stars.

Subject headings: line formation — radiative transfer — Sun: atmosphere

I. INTRODUCTION

Spatially resolved observations of the solar spectrum provide constraints on models for spectral line formation that are not available in spectra from other stars. This paper exploits such solar observational constraints to investigate the formation of Fe II lines in stellar atmospheres. Fe II line formation is of special interest because so many objects show Fe II lines in emission. A recent ESA workshop devoted to Fe II emission lines has been summarized in 1979, *Nature*, **282**, 559.

In particular, we discuss the formation in the solar spectrum of the weak Fe II λ3969.4 intersystem doublet line ($a\ ^4P_{5/2}$–$z\ ^6D^o_{7/2}$ and $a\ ^4P_{3/2}$–$z\ ^6D^o_{7/2}$, multiplet 3), which lies 0.9 Å redward of the center of the strong Ca II H resonance line. This line belongs to the class of *solar-disk emission lines* that appear in the extended wings of Ca II H and K. Spatially averaged profiles of these lines reverse from absorption into emission over the local background close to, but still inside, the solar limb. The limb emission of λ3969.4 was discovered by Evershed (1929). The line was attributed to Eu II or the wing of an Fe I line by Thackeray (1935, 1936), to Er II by Jensen and Orrall (1963), and finally to Fe II by Engvold and Halvorsen (1973) and Stencel (1973). As noted by Engvold and Halvorsen (1973), the λ3969.4 line then differs from the majority of the limb emission lines in the wings of H and K, which are due to rare earth ions.

The rare earth lines appear in emission near the limb because they are interlocked to rare earth lines outside H and K (Canfield 1971*b*). The latter lines themselves have raised NLTE source functions, as a result of the predominance of scattering in these optically thin, but resonance-like, transitions (Canfield 1969, 1971*a*). The rare earth limb emission is therefore due to extra photons that are scattered from *deep photospheric* layers.

The Fe II λ3969.4 line is formed differently. Lites (1974) proposed that the limb emission of this line is of *chromospheric* origin. He pointed out that the λ3969.4 doublet shares its upper levels with various lines of the strong Fe II resonance multiplet (UV 1, λλ2611.9, 2617.6, 2585.9, 2598.4, 2631.0, and 2631.3). A model Fe II computation showed that the formation of λ3969.4 is controlled by the UV lines. The model predicted intense self-reversed emission cores for these lines, which would provide a chromospheric photon source. Downward photon diffusion would pump the upper level near the temperature minimum, causing the observed limb emission of λ3969.4.

[1] On leave from the Astronomical Institute, Sterrewacht "Sonnenborgh," Utrecht, The Netherlands.

[2] Operated by the Association of Universities for Research in Astronomy, Inc., under contract AST 78-17292 with the National Science Foundation.

Subsequently, Canfield and Stencel (1976) compared the spatial intensity variation of λ3969.4 near the solar limb with that of a nearby Ce II limb emission line. The latter shows only weak spatial intensity variation, in accordance with Canfield's (1969) rare earth emission mechanisms which imply line-source function control through radiation fields that are averaged over a large volume. On the other hand, λ3969.4 shows very strong spatial intensity variation. Canfield and Stencel (1976) concluded that its identification is correct and that the line should be a useful diagnostic of stellar chromospheres.

Finally, a comprehensive catalog of H and K solar-limb emission lines by Rutten and Stencel (1980) shows that there are four more Fe II limb emission lines superposed on H and K: λλ3938.3, 3945.2, 3981.6 also of multiplet 3, and λ3974.2 of multiplet 29 ($b\,^4P$–$z\,^4P^o$); these lines all show strong, spatially correlated intensity variations.

Stellar emission lines in the wings of H and K have been studied by Stencel (1977). He found some *solar-limb* emission lines also to be in emission in the *flux spectra* of luminous cool stars, and for several of these he found a relation between line width and luminosity analogous to the Wilson-Bappu relation for the H and K emission cores. Such width-luminosity correlations are probably present only in Fe II–type lines (Rutten and Stencel 1980).

The Fe II–type emission lines in the H and K wings should then be valuable diagnostics of stellar chromospheres, provided that their emission is indeed of chromospheric origin. Two observations have led us to reexamine this problem. First, solar observations with high spatial resolution (Fig. 1, Pl. 2) show that the spatial intensity variation in Fe II λ3969.4 is *not* correlated with the chromospheric structure observed in the nearby Ca II H_2 emission features. Instead it is highly correlated with the *local* H-wing background, which is photospheric in origin. This observation will be discussed in detail in § II. Second, recent atlases of the solar near-UV spectrum do *not* show the intense reversals of the Fe II resonance lines required by Lites's (1976) mechanism. The unexpected absence of emission cores in these lines, in contrast to the Mg II and Si II resonance lines which are of similar abundance, ionization potential, and oscillator strength, has been pointed out earlier (Athay and Lites 1972; Huber 1974); this unsolved problem is obviously important for the formation of λ3969.4.

Section III presents Fe II model computations which concentrate on the formation of the UV resonance lines. These computations show that the pumping is due to UV line-wing photons from the deep photosphere rather than line-core photons from the chromosphere. In § IV we discuss the effects of coherent scattering and of atmospheric inhomogeneities. We find that the pumped Fe II lines respond sensitively to *deep* photospheric structure and that their solar spatial intensity variations are due to photospheric fine structure rather than to chromospheric inhomogeneities. Section V presents implications for Fe II line formation and for diagnostics of the inhomogeneous structure of the solar atmosphere and of the atmospheres of other cool stars.

II. SPATIAL INTENSITY VARIATION OF Fe II λ3969.4

Fe II λ3969.4 is present in spectrograms with high spatial and spectral resolution made with the Vacuum Tower Telescope at Sacramento Peak Observatory, as part of the HIRKHAD program (Beckers *et al.* 1972). A selection of these spectrograms is found in Figure 1, which shows several remarkable properties of the *fine structure* of λ3969.4. The intensity fluctuations in the line are much larger than those in any other weak line present, including the Ce II λ3967.0 limb emission line; they are also much larger than the fluctuations in the adjacent H-line wing. At disk center ($\mu = 1$) the line often appears in absorption, especially in the dark H-wing "threads." In bright H-wing threads the line is often invisible, but even at disk center it is occasionally seen in emission. At $\mu = 0.38$ the line generally appears in emission in the bright threads, and in absorption in the dark threads; there are many places where no line can be seen. At $\mu = 0.24$ the line appears in emission in the bright threads, and it is absent or in weak absorption in the dark threads.

The spectrograms show a strong spatial correlation between the intensity variations of λ3969.4 and those of the adjacent H-wing background: the line shows the background structure, but in an enhanced fashion. Moreover, the spectrograms show *no* strong spatial correlation between the intensity fluctuations of λ3969.4 and the chromospheric structure seen in the *core* of the Ca II H line, except at points where intense H-wing threads connect to core emission knots. These intense threads probably correspond to the phenomena called "whiskers" by Beckers and Artzner (1974). Table 1 quantifies the degree of spatial correlation between fine structures at different wavelengths across the line in terms of cross-correlation coefficients, determined from microphotometry of the spectra. The coefficients are very high for the spatial correlation between λ3969.4 and its adjacent background, and they are low for the spatial correlation between λ3969.4 and the chromospheric H_2 emission. Further, both H_ϵ and Ce II λ3967.0 are also each highly correlated with their H-line wing background and only weakly correlated with chromospheric structure.

The following are thus basic properties of the Fe II λ3969.4 line:

i) Its spatially averaged profile turns from absorption into emission well inside the limb.

ii) Its spatial intensity variation is very pronounced, and both absorption and emission features can be found over the whole disk.

iii) Its spatial intensity variation correlates strongly with the structure of the adjacent H-wing background, and not with the structure in the H-line core.

TABLE 1

CROSS-CORRELATION COEFFICIENTS

	I(background)			I(H_2 peak)		
	$\mu = 1.0$	$\mu = 0.38$	$\mu = 0.24$	$\mu = 1.0$	$\mu = 0.38$	$\mu = 0.24$
I(Fe II λ3969.4)	0.98	0.98	0.95	0.38	0.43	0.22
I(H_ϵ λ3970.1)	0.84	0.81	0.80	0.24	0.23	0.32
I(Ce II λ3967.0)	0.99	0.99	0.99	0.34	0.33	0.09

NOTE.—I(background) is measured in the H-line wings adjacent to each spectral line.

iv) Its spatial intensity variation is enhanced relative to the variation of the adjacent background.

III. Fe II MODEL COMPUTATIONS

a) Outline of Computations

We model the NLTE formation of the Fe II UV resonance lines and λ3969.4 under the assumptions of a simplified atomic model, a standard one-dimensional model atmosphere, and complete redistribution in angle and frequency. Within these assumptions, and with the available spatially averaged solar-atlas data as input, we cannot derive a definitive model, because insufficient observational and experimental constraints are available to permit precise determination of the many parameters. Our modeling should therefore be regarded as exploratory in character.

b) Solar Line Profiles

The partial Fe II Grotrian diagram (Fig. 2) shows the lines included in this study. In addition to lines of multiplets UV 1 and 3 we include lines from multiplets 1 and 40 for which solar data are available and which share $z\ ^6D^o_{7/2}$ as upper level. Figure 3 demonstrates that λ3255.9 of multiplet 1 is formed anomalously compared with neighboring lines. The other members of this multiplet similarly show extreme weakening toward the limb.

The best available observations of the lines of multiplet UV 1 are those of Kohl, Parkinson, and Kurucz (1978). Their low-dispersion tracings (p. 35) show how the 13 overlapping lines of this multiplet dominate the 2575–2635 Å region. These lines have no discernible reversals. The λ2585.9 line is the least blended and the only one for which the wings can be traced out to $\Delta\lambda = \pm 0.5$ Å. We used the disk-center and limb ($\mu = 0.23$) profiles of this line and fitted a local "continuum" through the highest intensity points present, at 2581.3 and 2638.0 Å.

Profiles of the other lines were taken from various sources, in the absence of a comprehensive solar-spectrum atlas (see Rutten 1979): λ3969.4 ($\mu = 1$ and $\mu = 0.2$) from the scans of Engvold and Halvorsen (1973), λ3255.9 ($\mu = 1$) from Brault and Testerman (1972), λ6516.1 ($\mu = 1$) from Delbouille, Roland, and Neven (1973), and for $\mu = 0.2$ from Brault and

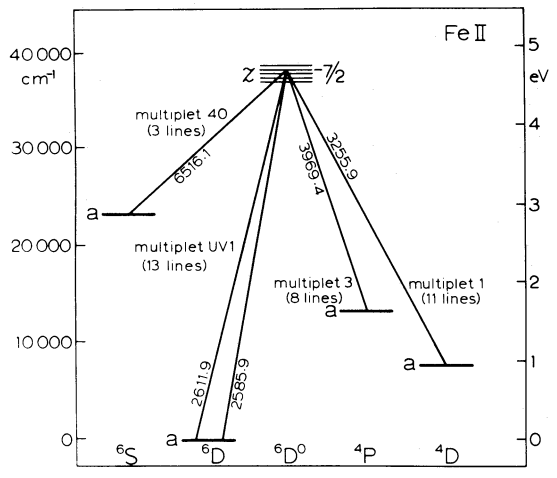

FIG. 2.—Partial Grotrian diagram for Fe II, showing the lines computed in this study. The fine structure of the z^6D^o term is indicated schematically, and the total number of lines per multiplet are specified.

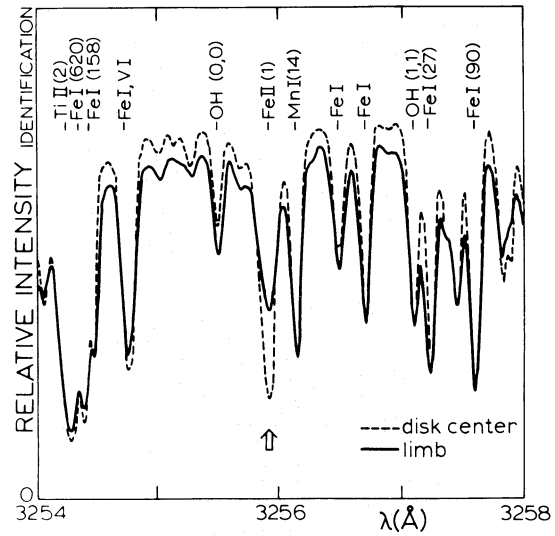

FIG. 3.—Superposed disk-center and limb scans from Brückner's (1960) solar UV atlas near 3255 Å. Fe II λ3255.9 (multiplet 1) is prominent because of anomalous limb darkening.

TABLE 2

Fe II MODEL

Wavelength	Multiplet	Transition	Oscillator Strength	Radiative Damping (s^{-1})
2611.9	UV 1	$a\ ^6D_{7/2}$–$z\ ^6D^o_{7/2}$	0.35	7×10^8
2585.9	UV 1	$a\ ^6D_{9/2}$–$z\ ^6D^o_{7/2}$	0.18	7×10^8
3255.9	1	$a\ ^4D_{5/2}$–$z\ ^6D^o_{7/2}$	1×10^{-4}	7×10^8
3969.4	4	$a\ ^4P_{5/2}$–$z\ ^6D^o_{7/2}$	6×10^{-5}	7×10^8
6516.1	40	$a\ ^6S_{5/2}$–$z\ ^6D^o_{7/2}$	1×10^{-4}	7×10^8

Testerman (1972). These profiles are all given relative to the local continuum only.

c) *Model Atom and Model Atmosphere*

The model of the Fe atoms contains the three lowest terms of Fe I ($a\ ^5D$, $a\ ^5F$, and $a\ ^3F$), the 11 lowest terms of Fe II ($a\ ^6D$, $a\ ^4F$, $a\ ^4D$, $a\ ^4P$, $a\ ^2G$, $b\ ^4P$, $a\ ^4H$, $b\ ^4F^o$, $a\ ^2P$, $a\ ^2H$, and $a\ ^2D$—the last three being combined as one representative term), the $a\ ^6S_{3/2}$ and $z\ ^6D^o_{7/2}$ levels, and the Fe II continuum level. The terms were specified as single levels (effective multiplets) with the average excitation energy of the term and its total statistical weight. Fe I and all low metastable levels of Fe II were included because the large number of these low-lying levels makes Fe II different from Mg II and Si II. Collisional excitation, de-excitation, ionization, and recombination processes were included for all terms, with cross sections set equal to πa_0^2 where a_0 is the first Bohr orbit radius.

The lines are specified in Table 2. Their level populations were derived from the term populations by assuming detailed balance for the fine-structure levels. We consider only transitions to the $z\ ^6D^o_{7/2}$ level, neglecting the $z\ ^6D^o_{5/2}$ level, from which the other component of the λ3969.4 doublet originates, and the other $z\ ^6D^o$ fine-structure levels. Of multiplet UV 1 we include λ2611.9 (7/2–7/2) because it is the strongest of the three UV 1 transitions from $z\ ^6D^o_{7/2}$, and λ2585.9 (9/2–7/2) because it is the best observed.

Oscillator strengths of lines of multiplet UV 1 have been measured by Assousa and Smith (1972) and by Huber (1974). Their values of λ2585.9 differ by a factor of 2; so we treat this oscillator strength as a free parameter. The oscillator strengths of the lines of the other multiplets are also treated as free parameters. We assume that the *ratios* of the oscillator strengths of λ2611.9, λ2585.9, and λ2631.3 as measured by Huber (1974) are correct. Radiative damping is taken to be 1.5 times the sum of the radiative transition probabilities of these three lines; the increase by 50% serves as a correction for other decay paths from $z\ ^6D^o_{7/2}$ that were neglected. Van der Waals damping is computed with the Bates-Damgaard approximation, neglecting the lower levels and multiplying the result with a correction factor of 3 (see Holweger and Müller 1974). Radiative processes for other transitions are neglected except for photoionization and recombination. These are included as fixed rates, specified by radiation temperatures taken constant above the Eddington-Barbier depth $\tau_\nu^c = 1$.

We employ the HSRA atmosphere (Gingerich *et al.* 1971) and an isotropic microturbulence model shown in Figure 4, from Vernazza, Avrett, and Loeser (1976).

Additional quasi-continuous opacities are included for the two UV lines and for λ3969.4. For the UV lines, we multiply the computed continuous opacity by a factor of 3, determined by fitting the computed continuous intensity to the observed "local" continuum level at disk center. This procedure corrects for the dense line haze present at these wavelengths, on the assumption that the depth dependence of the line-haze opacity mimics the depth dependence of the continuum opacity. This assumption is roughly verified by the fact that the observed limb darkening of the local continuum is well reproduced by the model. For λ3969.4 the underlying wing opacity of the Ca II H line has to be added. We use the approximation by Shine

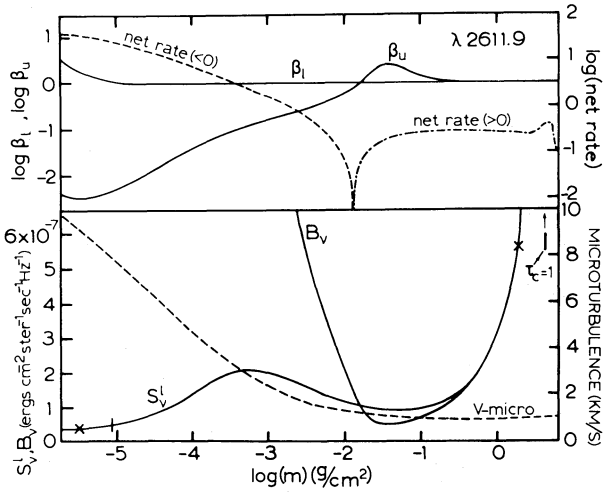

FIG. 4.—Results for λ2611.9—*Abscissa:* logarithm of mass column density; *top:* NLTE departure coefficients of the upper and lower levels (*solid lines*) and net radiative upward rate (positive: *dot-dashed line;* negative: *dashed line*); *bottom:* Planck function and line source function (*solid lines*); macroturbulence distribution (*dashed line*). The Eddington-Barbier locations where the radial continuum optical depth and the total optical depth at line center equal the direction cosine ($\tau = \mu$) are indicated by ticks for $\mu = 1$ and by crosses for $\mu = 0.23$.

and Linsky (1974*a*) scaled over the H/K = 0.5 *gf*-value ratio. This approximation satisfactorily reproduces the observed absolute intensity near λ3969.4 derived from Pasachoff's (1971) calibration.

d) Computational Methods

The coupled radiative-transfer equations and multilevel statistical equilibrium equations are solved using a multilevel version of the linearization scheme described by Rybicki (1970). The code is similar to that of Auer and Heasley (1976) and employs the successive overrelaxation iteration procedure. The HSRA model atmosphere is sampled at 50 depth points, and the five lines are sampled at a total of 106 frequency points, including their full wings. Convergence to 0.1–1% precision is usually reached in three iterations.

Computed profiles were fitted to the observations in the following manner. Lites's (1974) value of the Fe abundance is adopted (Fe/H = 1.5×10^{-5}). The λ2585.9 oscillator strength is then determined by fitting the observed wings at disk center, varying the λ2611.7 oscillator strength and the radiative damping of all lines concurrently. The subordinate lines are then fitted by varying their oscillator strengths, concentrating on the observed central intensity at disk center. The resulting parameter values are given in Table 2.

Extensive trial computations were performed for other values of the Fe abundance, collisional cross-sections, van der Waals damping constants, and for other microturbulence models. These show that the UV line oscillator strengths and radiative damping widths are the most sensitive parameters. For different values of the other parameters the fitting procedure leads to numerically different results, but to the same basic source-function structures and pumping mechanisms as presented below.

e) Results

Figures 4 and 5 show the line-source functions and the computed profiles for the five lines. We discuss first the *source functions*. All low levels are in Boltzmann equilibrium throughout the photosphere and low chromosphere. The lines therefore have similar opacity distribution with height and can be discussed in terms of their source functions. The population of the shared $z\,^6D^o_{7/2}$ upper level simultaneously sets the deviations from LTE in all five line-source functions. A good measure of these deviations is therefore the upper-level departure coefficient β_u, defined here as the ratio of the actual population to the LTE Boltzmann-Saha population normalized to the total number density of Fe, rather than to the next ion's population, as in the customary Menzel definition (see Wijbenga and Zwaan 1972). The line-source function S_ν^l is very closely given by

$$S_\nu^l(h) = \beta_u(h) B_\nu[T_e(h)] , \qquad (1)$$

where B_ν is the Planck function defined by the electron temperature T_e at height h. Hence we have source-function equality in all lines, in the sense of population equality (see Athay 1972, p. 101). However, note from Figure 5 that the actual height variation of the line-source functions changes from line to line, because of differences in Planck function steepness over the spectrum. For example, at the temperature minimum the source function S_ν^l of λ2611.9 has a minimum (Fig. 4), while that of λ6516.1 (Fig. 5) has a prominent peak.

We find, as did Lites (1974), that the population of $z\,^6D^o_{7/2}$ is completely dominated by the UV lines: the transition rates in the other lines are negligible. Hence the departures from LTE in all subordinate lines are controlled by UV pumping. However, in contrast to the earlier result, we find here that this pumping occurs in the *photosphere*. The net radiative rates of the UV lines are shown in Figure 4. These rates lead to overpopulation of the $z\,^6D^o_{7/2}$ level remarkably deep in the atmosphere. Above the temperature minimum where the presence of an optical boundary leads to increasing photon loss, the net rate reverses sign. The magnitude of the negative net rate increases outward, and the weak collisional coupling to the chromospheric temperature rise produces only a weak maximum in the chromospheric line-source function.

There is *no* downward diffusion of photons from the chromosphere to layers below the temperature minimum. This is demonstrated by deleting the chromospheric temperature rise of the HSRA and replacing it by a constant temperature equal to the minimum value of 4170 K. As Figure 6 shows there is no change in the photospheric part of the λ3969.4 source function.

The extra photons below the temperature minimum are instead supplied by the high intensity in the wings of the UV lines in deep photospheric layers. As indicated in Figure 4, the UV continuum is formed quite deep and, since near 2600 Å the mean intensity J_ν is already larger than B_ν at that height (see Vernazza, Avrett, and Loeser 1976, p. 44), a strong source of wing photons is available. *It is the resonance scattering in the high-intensity wings, redistributed over the ultraviolet line profiles, that raises S_ν^l in the layers below the temperature minimum.*

The *profiles* shown in Figure 5 fit the observations satisfactorily, given the exploratory nature of this investigation. We note, however, that the computed subordinate lines are too weak in their far wings and that λ3255.9, λ6516.1, and the inner wings of λ2585.9 are too deep near the limb. The computed limb darkening in these lines does not fully reproduce the observed anomalous limb darkening (Fig. 4), which implies that our model underestimates the amount of departure from LTE in the photosphere. In § IV we suggest that partially coherent scattering may lead to a larger photospheric overpopulation of the $z\,^6D^o_{7/2}$ level.

The computed UV lines have weak reversals, exaggerated in Figure 5 by the log-log scales, which could be easily obliterated by macroscopic velocities. Our fit of the λ2585.9 wings thus leads to a formation model

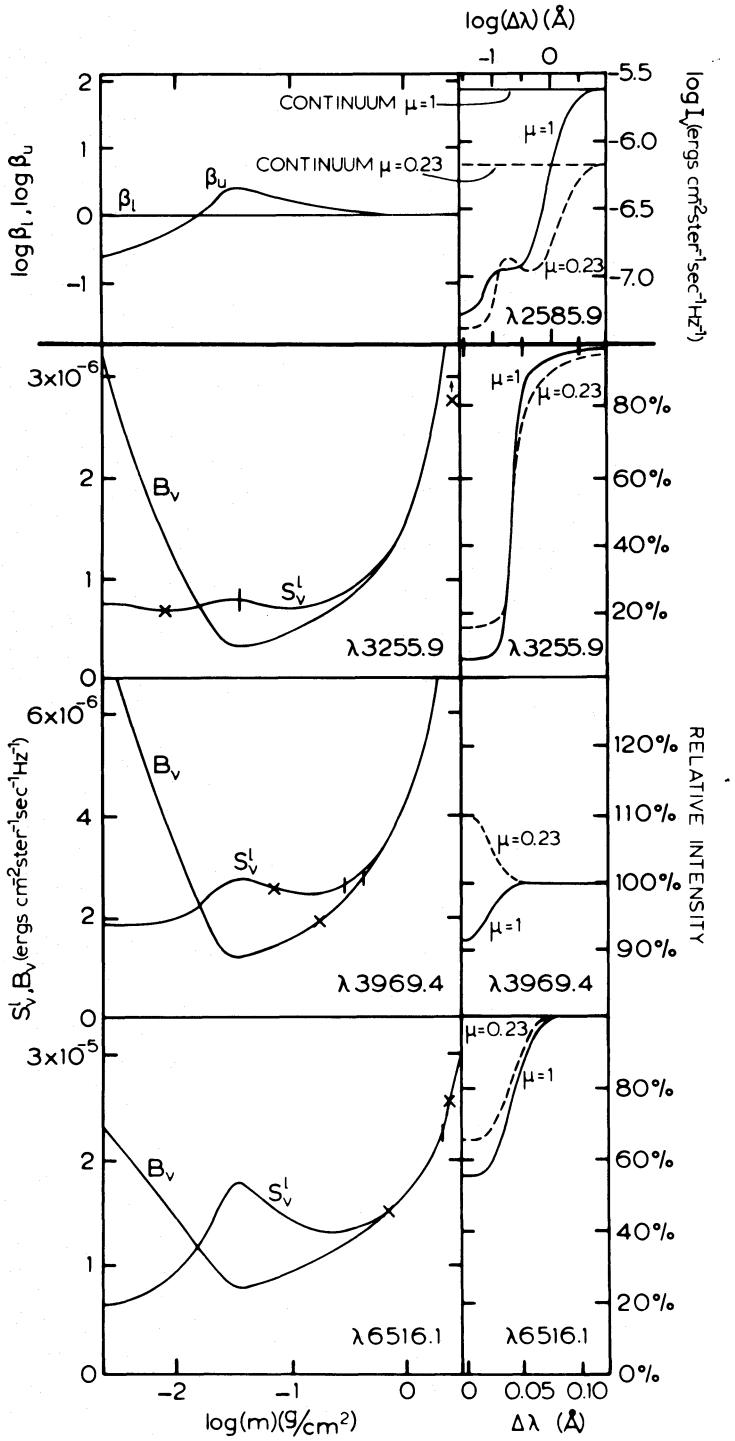

FIG. 5.—Results for λλ2585.9, 3255.9, 3969.4, and 6516.1—*left:* NLTE departure coefficients (*top*) and resulting line source functions. Ticks and crosses denote Eddington-Barbier locations for $\mu = 1$ and $\mu = 0.23$; *right:* computed line profiles for $\mu = 1$ and $\mu = 0.23$; *abscissae:* wavelength separation from line center in Å, logarithmic for λ2585.9; *ordinates:* logarithm of absolute intensity for λ2585.9, relative intensity (scaled to continuum = 100) for the other lines.

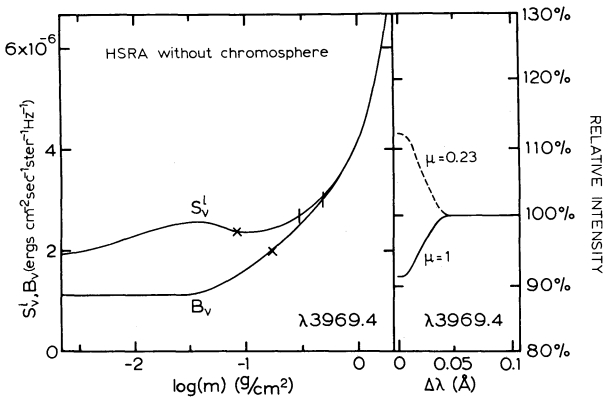

FIG. 6.—Results for λ3969.4 for a model without chromosphere, labeled as in Fig. 5.

which is *not* in conflict with the observed absence of self-reversals in the UV line cores.

Finally, the model explains the spatially averaged properties of λ3969.4, as shown by Figure 5. The height of formation of this weak line and of its H-wing background are raised enough that the overpopulation of the upper level results in emission near the limb. The computed line-center intensity fits the observed value, both in absorption at $\mu = 1$ and in emission at $\mu = 0.23$. The no-chromosphere model of Figure 6 shows even stronger emission, but this is because of the slight lowering of the H-line background by the elimination of its chromospheric contribution.

IV. DISCUSSION

a) Values of Oscillator Strengths

Our λ2585.9 oscillator strength is similar to Huber's (1974) value. For λ3255.9 (our value 1×10^{-4}) Grasdalen, Huber, and Parkinson (1969) measured 2.3×10^{-4} with a shock tube. For λ6516.1 (our value 1×10^{-4}) Phillips (1979) derives 1.1×10^{-4} from a solar curve of growth procedure. Finally, our oscillator strength for λ3969.4 (6×10^{-5}) agrees with the value calculated by Kurucz and Peytremann (1975; 1.8×10^{-5}). We note, however, that their value for λ6516.1 is five orders of magnitude wrong—see Phillips (1979). These parameters, while model dependent, are thus not in conflict with previous results.

b) Coherency Effects

Partially coherent scattering is neglected in our model. However, coherency effects may be present in the formation of the Fe II lines, and they are undoubtedly present in the formation of the Ca II H-wing background near λ3969.4. We discuss these effects separately for the various lines.

i) *Coherency in the* Fe II *resonance lines.*—Since all our lines share the same upper level and have sharp lower levels, our Fe II model ion is similar to the Ca II model ion discussed by Milkey, Shine, and Mihalas (1975). In the absence of perturbations of the excited state, photons exchange between the resonance lines and the subordinate lines without loss of coherency. We illustrate the effects of partial coherency by presenting in Figure 7 results for the case of *completely* coherent scattering at all wavelengths in the resonance lines. This extreme example leads to marked frequency dependence of the line-source function. It shows that the potential effects of coherency are very large. It also shows in which sense, qualitatively, such effects will change the Fe II line formation when they are present. Chromospheric coherency in the core will lead to intense self-reversals; coherency just below the temperature minimum in the innermost wings will lead to deep secondary intensity minima; coherency in deeper layers in the outer wings will lead to high-intensity wings. The core and inner wing effects are present in the Mg II *h* and *k* and Ca II H and K lines (Milkey and Mihalas 1974; Vardavas and Cram 1974; Shine, Milkey, and Mihalas 1975); the far-wing intensity increase is displayed by Ba II λ4554 near the limb (Rutten and Milkey 1979).

Loss of coherency will, in our atomic model, only be accomplished through Doppler redistribution in the

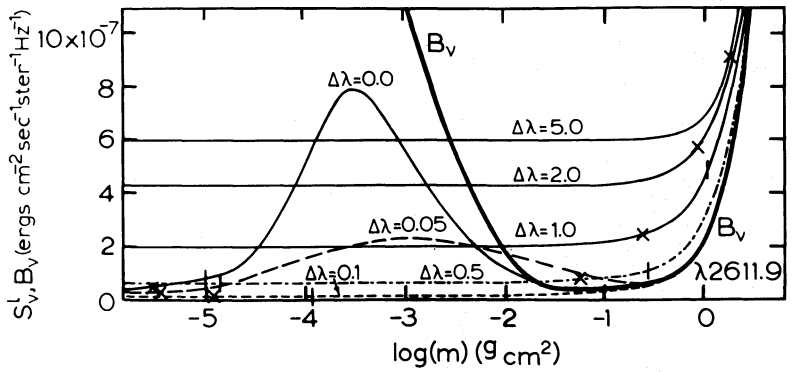

FIG. 7.—Wavelength-dependent line source function of λ2611.7 for the assumption of completely coherent scattering. The various components are indicated by their wavelength separation from line center in Å. Ticks and crosses denote Eddington-Barbier locations for $\mu = 1$ and $\mu = 0.23$.

line cores and through collisional redistribution in the damping wings. The former occurs especially in the chromosphere (large microturbulence), the latter in the deep photosphere (frequent collisions). However, the *real* Fe atom differs from our model in having a highly complex resonance multiplet of 13 transitions, connecting five fine-structure upper levels rather than one. Many of these lines overlap, giving emitted photons a choice, e.g., between the wing of one line and the core of another. Collisional exchange between the fine-structure levels will also cause redistribution. These combined effects cannot be estimated easily, but we suspect that the redistribution due to this complex fine structure will be extensive. Complete redistribution (CRD) may even be a fair assumption for the Fe II resonance lines, especially for their cores.

ii) *Coherency in the* Fe II *subordinate lines.*—The source functions of subordinate lines with metastable lower levels can be very sensitive to partial redistribution (PRD) in interlocked resonance lines. This effect is prominent in the weak Ba II $\lambda\lambda$4554–5854 line pair (Rutten and Milkey 1979). In Fe II, partially coherent scattering in the UV line wings below the temperature minimum would influence the subordinate lines seen near the limb. Their observed anomalous limb darkening, not fully reproduced by our CRD model, may be influenced by such effects.

iii) *Coherency in the* Ca II H-*wing background near* λ3969.4.—We employ the simple approximation of additional quasi-continuous opacity to account for the local H-line wing near the Fe II λ3969.4 line. This procedure is not correct, because at this wavelength the Ca line is formed by partially coherent scattering. However, observations show that the H-wing coherency plays no role in the spatial intensity variation of λ3969.4: the other three lines of multiplet 3 found by Rutten and Stencel (1980) show *exactly* the same behavior near the limb, although they are located far out in the H- and K-line wings where these are formed in LTE. The behavior of λ3969.4 is definitely a general property of Fe II subordinate lines and not due to peculiarities of partially redistributed scattering in the Ca II resonance line wings.

c) *Inhomogeneities*

We have employed a one-dimensional model to explain the spatially averaged behavior of the Fe II lines. In reality, as shown by Figure 1, the emission of λ3969.4 consists almost exclusively of fine-structure knots. Just as in the plane-parallel model, the line-source functions in the inhomogeneities are controlled by the inhomogeneous source functions of the UV lines. Because spatial averaging over fine structure in temperature leads to different weighting of the resulting UV intensity variation from that of the visible intensity variation, our mean model represents only a coarse approximation (Wilson and Williams 1970).

We now turn to the properties (ii)–(iv) of λ3969.4 formulated at the end of § II. Since we presently have no *physical* interpretation of the threads seen in Figure 1 in the local wing of H and enhanced in λ3969.4, we limit our discussion to the differences between two models, respectively, of *chromospheric* and *photospheric* inhomogeneities. These models are schematic and are not meant to represent quantitative descriptions of solar inhomogeneities.

i) *Plage model.*—Figure 8 shows the consequence of replacing the HSRA atmosphere by one of the plage models of Shine and Linsky (1974*b*, model 2-C). This is a typical model of a chromospheric inhomogeneity, in which the deviation from the mean (or quiet) atmosphere *increases* with height from the deep photosphere outward. It leads to intense self-reversals in the Fe II UV lines, which is not surprising since this model is designed to explain enhanced Ca II H and K emission in plages. Both the λ3969.4 intensity and the H background are brighter than in the quiet Sun model; the increases are similar in size.

ii) *Overshooting granule model.*—Figure 8 also shows the effect of raising the temperature of the HSRA in the deep photosphere by 150 K. The temperature excess decreases with height, reaching zero just below the temperature minimum. This is a schematic model of a photospheric inhomogeneity of which the differences with the mean atmosphere *decrease* with height (see Nelson and Musman 1977). This model does not change the cores of the Fe II UV lines, nor of the Ca II H and K lines. Both the λ3969.4 intensity and the local H-wing background are again brighter than the HSRA values, but in this case the line intensity increases more than the background intensity near the limb. A cooler "inter-granular" model with a deficit of 150 K in the deep photosphere leads similarly to enhanced *darkening* of the λ3969.4 line, without affecting the H-line core.

These results may be understood in terms of the source function structure of λ3969.4 shown in Figure 8 and the indicated Eddington-Barbier locations for the line and the H-wing background. The source function of λ3969.4 is controlled by the radiation field in the UV resonance lines, which overpopulates the upper level below the temperature minimum through pumping by UV-wing photons from the deep photosphere. In contrast, the H background is controlled locally. We thus have a line whose intensity is controlled by a radiation field formed deeper than its adjacent "continuum"!

The λ3969.4 observational constraints (ii)–(iv) of § II can thus be explained with the granular-type model occurring in discrete, small-scale patches over the solar disk. A similar application of the plage-type model lead instead to cospatial strong Ca II H_2 core emission and enhance the H-wing background as much as the λ3969.4 line in the hotter elements.

We conclude that the formation of the Fe II H- and K-limb emission lines is due to pumping through the interlocked UV resonance lines by *photospheric* UV photons. This mechanism is similar to Canfield's (1971*b*) mechanism for the rare earth H- and K-limb emission lines, which are also due to interlocking to

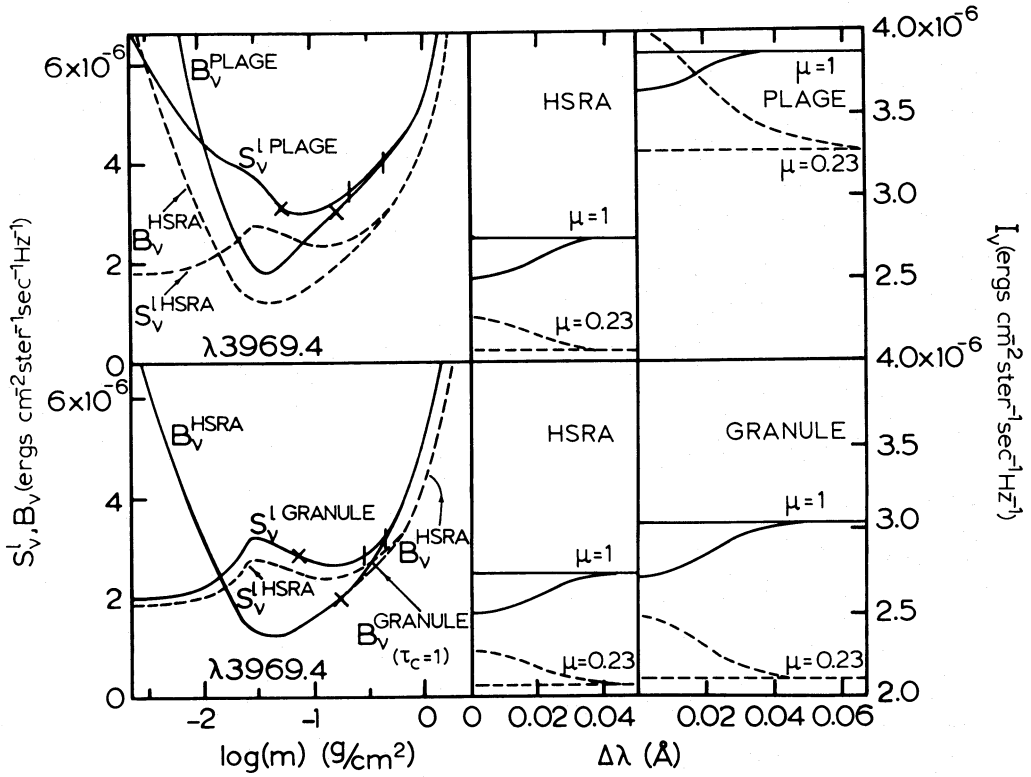

FIG. 8.—Results for λ3969.4 for a chromospheric inhomogeneity (plage) and for a photospheric inhomogeneity (granule)—*left:* Planck functions and line source functions (labeled as in Fig. 5); *right:* computed line profiles. Ordinates are linear absolute intensity.

sources of photospheric photons. But in that case, the sources are optically thin resonance lines in the same wavelength region, while for Fe II the sources are optically thick resonance lines in the UV. This difference leads to the extraordinary difference between these two types of H and K emission lines in their intensity response to photospheric inhomogeneities.

V. IMPLICATIONS AND PROSPECTS

a) *Other* Fe II *Lines*

We have shown that *all* solar subordinate lines with $z\ ^6D^o_{7/2}$ as upper level have UV-pumped suprathermal source functions in the photosphere. Another interesting line which we did not include for lack of center-to-limb observations is the Fe II λ2797.04 line (multiplet 32, $a\ ^4F$–$z\ ^6D^o_{5/2}$; Allen and McAllister 1977) which lies 1.6 Å to the red of the Mg II *k* line. It will be formed similarly to λ3969.4, but at greater height in the atmosphere.

There are many other subordinate Fe II lines that may be formed out of LTE in a manner similar to our examples of multiplets 1, 4, and 40. The pattern shown in Figure 3, of strong resonance-like UV transitions connectiong well-populated low levels to upper levels that are shared by many weaker lines in the visual, is a characteristic pattern of the Fe II spectrum. The deviations from LTE will be less obvious than for λ3969.4 with its disk emission. For other lines anomalous limb darkening, as shown in Figure 3, can serve as an observational indication of such departures from LTE, as can the behavior of the lines at the extreme solar limb (see discussion in Rutten and Stencel 1980 of the line list by Pierce 1968).

b) Fe II *Lines as Solar Diagnostics*

The behavior of λ3969.4, in relation to the threads observed in the adjacent H wing, provides a sensitive diagnostic of photospheric fine structure. We cannot state at present whether the threads are of convective, oscillatory, or magnetic origin; the extra constraints furnished by λ3969.4 will help determine their nature. We expect that the other UV-controlled subordinate lines also have enhanced sensitivity to temperature variations. For the application of these diagnostics a detailed PRD analysis of multiplet UV 1 will be a necessary and interesting endeavor.

c) Fe II *Lines as Stellar Diagnostics*

We cannot resolve stellar surface detail and therefore have to transform our resolved solar results into spectroscopic diagnostics of stellar *flux* spectra—which, however, add information by showing changes from star to star. In late-type stars, strong emission is often observed in the Ca II H and K cores. The peak

intensities can differ markedly for otherwise apparently identical stars at the same location in the H-R diagram and with the same emission-core *width* (Linsky *et al.* 1979). The core width, which is tightly correlated with luminosity (Wilson and Bappu 1957) is usually interpreted as a measure of the mean radial structure of the atmosphere (Jefferies and Thomas 1960); the emission *intensity* can be interpreted as measuring the chromospheric number density of discrete magnetic flux tubes (Zwaan 1977).

In this context, Stencel's (1977) discovery of width-luminosity correlations for weak H and K emission lines of cool giants, Rutten and Stencel's (1980) evidence that these are especially prominent in lines similar to λ3969.4, and our results for this line in the Sun lead to interesting diagnostic prospects. The comparison between our "plage" and "overshooting granule" models shows that solar emission in Fe II H- and K-wing emission lines *without concurrent* H *and* K *core emission* is to be interpreted as a result of the fine structure of the deep photosphere, while emission concurrent with strong H and K core emission results from chromospheric fine structure. For the Sun, "concurrent" means *cospatial*: our high-resolution solar observations show that the spatially averaged quiet-Sun emission of λ3969.4 toward the limb is due to fine structure in the deep photosphere: the emission would still be present if the Sun had no chromosphere at all.

For stars, it follows that concurrent brightening of the H and K cores and the Fe II UV-pumped emission lines in one star over another similar star indicates differences in *chromospheric* fine structure. Extra brightening of λ3969.4–type lines alone, without concurrent H and K brightening, indicates differences in *photospheric* inhomogeneous structure. This suggests that the pumped Fe II lines provide a third, independent diagnostic, in addition to the H and K emission core widths and strengths, which may serve to disentangle mean radial structure, chromospheric inhomogeneity, and photospheric inhomogeneity in late-type stars. It would be particularly useful to have high-quality stellar H and K spectra of a large sample of late-type stars to explore how the H and K–Fe II correlation changes from star to star, and also to have time series of spectra (over days, months, years) for a smaller sample of stars to see how the correlation changes with changing degree of stellar activity.

VI. CONCLUSIONS

The behavior of Fe II λ3969.4 over the solar disk is explained by an Fe II model based on observations of the λ2585.9 resonance line. Our main conclusions are:

i) Due to pumping by wing photons in the Fe II UV resonance lines, the intensity of λ3969.4 responds sensitively to photospheric structure at a greater depth than that to which the "continuum" background intensity responds.

ii) Quiet-Sun fine structure ("threads") in λ3969.4 and the adjacent H wing is due to photospheric inhomogeneities.

iii) The λ3969.4 line provides a valuable diagnostic into atmospheric fine structure, for the Sun and likewise for other cool stars.

iv) The observed absence of intense self-reversals in the cores of the Fe II UV resonance lines is adequately reproduced by our CRD formation model.

v) Many subordinate lines of Fe II will be formed out of LTE.

We are grateful for the opportunity to use the HIRKHAD observations, whose superb quality is due to the efforts of Drs. J. M. Beckers, D. R. Brown, and their collaborators at the Sacramento Peak Observatory. We are indebted to Dr. C. Zwaan for discussions, to Drs. A. G. Hearn and S. L. Keil for comments on the paper, to Mr. E. B. J. van der Zalm for help with the computations, and to the National Center for Atmospheric Research and Utrecht University for computer time. R. J. R. acknowledges a NATO Science Fellowship awarded by the Netherlands Organization for the Advancement of Pure Research (Z.W.O.).

REFERENCES

Allen, M. S., and McAllister, H. C. 1977, *Ap. J. (Letters)*, **218**, L137.
Assousa, G. E., and Smith, W. H. 1972, *Ap. J.*, **176**, 259.
Athay, R. G. 1972, *Radiation Transport in Spectral Lines* (Dordrecht: Reidel).
Athay, R. G., and Lites, B. W. 1972, *Ap. J.*, **176**, 809.
Auer, L. H., and Heasley, J. N. 1976, *Ap. J.*, **205**, 165.
Beckers, J. M., and Artzner, G. 1974, *Solar Phys.*, **37**, 309.
Beckers, J. M., Mauter, H. A., Mann, G. R., and Brown, D. R. 1972, *Solar Phys.*, **25**, 81.
Brault, J. W., and Testerman, L. 1972, *Kitt Peak Solar Atlas* 2942 *to* 10014 Å: *Preliminary Edition* (Tucson: Kitt Peak National Observatory).
Brückner, G. 1960, *Photometrische Atlas des nahen Ultravioletten Sonnenspektrums von* 2988 Å–3629 Å (Göttingen: Universitäts-sternwarte).
Canfield, R. C. 1969, *Ap. J.*, **157**, 425.
———. 1971*a*, *Astr. Ap.*, **10**, 54.
———. 1971*b*, *Astr. Ap.*, **10**, 64.
Canfield, R. C., and Stencel, R. E. 1976, *Ap. J.*, **209**, 618.
Delbouille, L., Roland, G., and Neven, L. 1973, *Photometric Atlas of the Solar Spectrum from* λ3000 *to* λ10000 (Liège: L'Institut d'Astrophysique).
Engvold, D., and Halvorsen, H. D. 1973, *Solar Phys.*, **28**, 23.
Evershed, J. 1929, *M.N.R.A.S.*, **89**, 566.
Gingerich, O., Noyes, R. W., Kalkofen, W., and Cuny, Y. 1971, *Solar Phys.*, **18**, 347.
Grasdalen, G. C., Huber, M. C. E., and Parkinson, W. H. 1969, *Ap. J.*, **156**, 1153.
Holweger, H., and Müller, E. A. 1974, *Solar Phys.*, **39**, 19.
Huber, M. C. E. 1974, *Ap. J.*, **190**, 237.
Jefferies, J. T., and Thomas, R. N. 1960, *Ap. J.*, **131**, 695.
Jensen, E., and Orral, F. Q. 1963, *Pub. A.S.P.*, **75**, 162.
Kohl, J. L., Parkinson, W. H., and Kurucz, R. L. 1978, *Center and Limb Solar Spectrum in High Spectral Resolution* 225.2 nm *to* 319.6 nm (Cambridge: Harvard-Smithsonian Center for Astrophysics).
Kurucz, R. L., and Peytremann, E. 1975, *Smithsonian Ap. Obs. Spec. Rept.*, No. 362.

Linsky, J. L., Worden, S. P., McClintock, W., and Robertson, R. M. 1979, *Ap. J. Suppl.*, **41**, 47.
Lites, B. W. 1974, *Astr. Ap.*, **33**, 363.
Milkey, R. W., and Mihalas, D. 1974, *Ap. J.*, **192**, 769.
Milkey, R. W., Shine, R. A., and Mihalas, D. 1975, *Ap. J.*, **199**, 718.
Nelson, G. D., and Musman, S. 1977, *Ap. J.*, **214**, 912.
Pasachoff, J. M. 1971, *Solar Phys.*, **19**, 323.
Phillips, M. M. 1979, *Ap. J. Suppl.*, **39**, 377.
Pierce, A. K. 1968, *Ap. J. Suppl.*, **17**, 1.
Rutten, R. J. 1979, in *Future Solar Optical Observations—Needs and Constraints*, ed. G. Godoli, G. Noci, and A. Righini, *Osservazione e Memorie* (Florence: Osservatorio Astrofisici di Arcetri), Vol. **106**, p. 221.
Rutten, R. J., and Milkey, R. W. 1979, *Ap. J.*, **231**, 277.
Rutten, R. J., and Stencel, R. E. 1980, *Astr. Ap. Suppl.*, in press.
Rybicki, G. B. 1970, *J. Quant. Spectrosc. Rad. Trans.*, **11**, 589.
Shine, R. A., and Linsky, J. L. 1974*a*, *Solar Phys.*, **37**, 145.
———. 1974*b*, *Solar Phys.*, **39**, 49.
Shine, R. A., Milkey, R. W., and Mihalas, D. 1975, *Ap. J.*, **199**, 724.
Stencel, R. E. 1973, *Solar Phys.*, **33**, 59.
———. 1977, *Ap. J.*, **215**, 176.
Thackeray, A. D. 1935, *Ap. J.*, **81**, 338.
———. 1936, *Pub. A.S.P.*, **48**, 330.
Vardavas, I. M., and Cram, L. E. 1974, *Solar Phys.*, **38**, 367.
Vernazza, J. E., Avrett, E. H., and Loeser, R. 1976, *Ap. J. Suppl.*, **30**, 1.
Wijbenga, J. W., and Zwaan, C. 1972, *Solar Phys.*, **23**, 265.
Wilson, O. C., and Bappu, M. K. V. 1957, *Ap. J.*, **125**, 661.
Wilson, P. R., and Williams, N. V. 1970, *Solar Phys.*, **26**, 30.
Zwaan, C. 1977, in *The Sun, a Tool for Stellar Physics*, ed. B. Caccin and M. Rigutti, *Mem. Soc. Ap. Italiana*, **48**, 3.

LAWRENCE E. CRAM: Sacramento Peak Observatory, Sunspot, NM 88349

BRUCE W. LITES: High Altitude Observatory, NCAR, P.O. Box 3000, Boulder, CO 80307

ROBERT J. RUTTEN: Sterrewacht "Sonnenborgh", Zonneburg 2, 3512 NL Utrecht, The Netherlands

PLATE 2

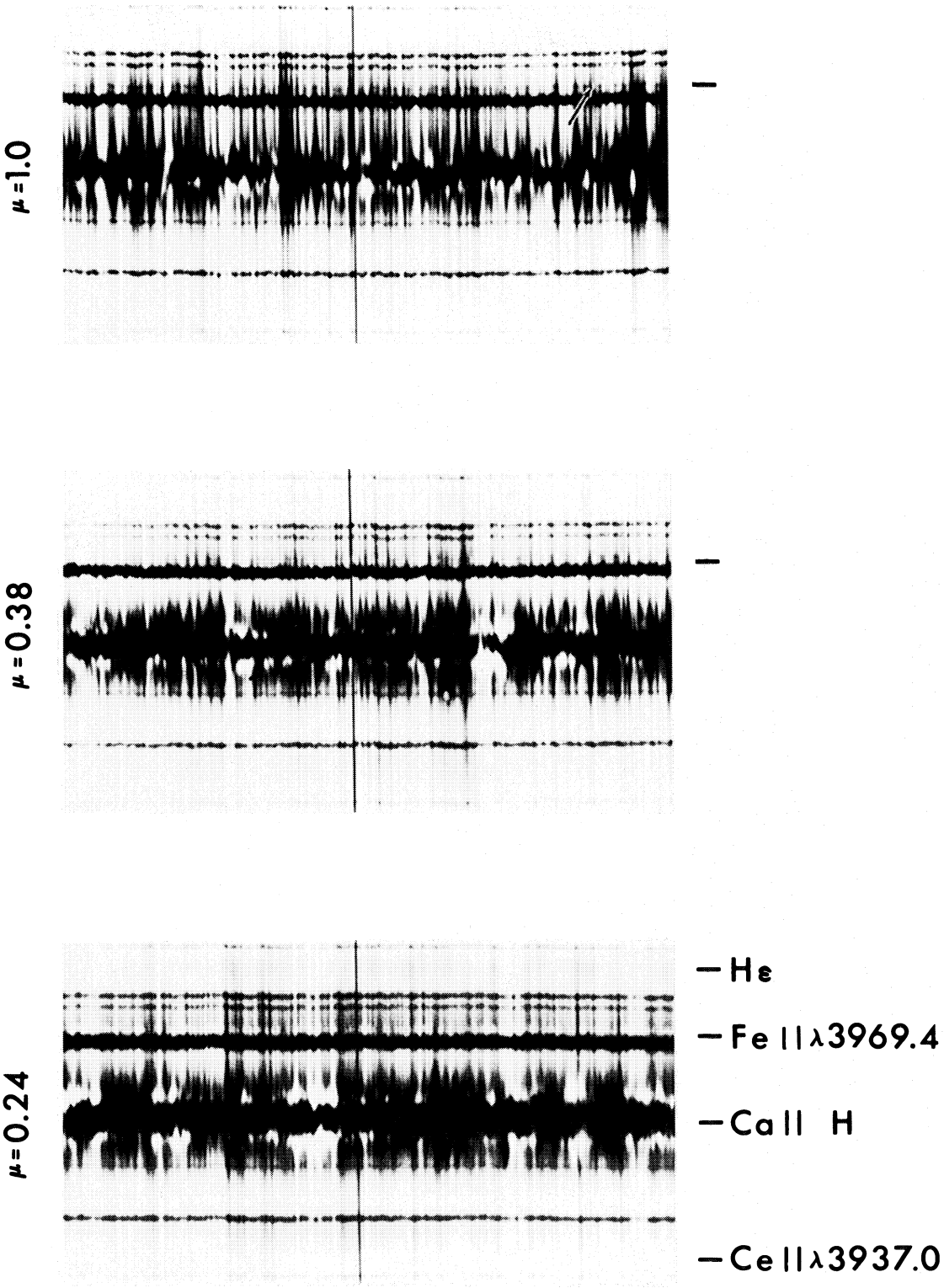

FIG. 1.—High-resolution spectrograms showing the solar center-to-limb variation of the core of Ca II H, hydrogen H_ϵ, and Fe II λ3969.4. The cosine of the viewing angle is μ. The striking spatial intensity variation of λ3969.4 along the slit is not correlated to the chromospheric structure seen in the core of the H line, but follows the *local* H-wing bright and dark threads in enhanced fashion. Even at disk center the line shows emission knots (*arrow*) (Sacramento Peak Observatory spectra).

CRAM et al. (*see* page 375)